Membrane fluidity adjusts the insertion of the transacylase PlsX to regulate phospholipid biosynthesis in Gram-positive bacteria

Diego E. Sastre[‡1], ◉ Luis G. M. Basso[§], Beatriz Trastoy[¶], Javier O. Cifuente[¶], Xabier Contreras[∥**‡‡],
◉ Frederico Gueiros-Filho[§§], Diego de Mendoza[¶¶], Marcos V. A. S. Navarro[‡], and Marcelo E. Guerin[¶∥2]

*From the ‡Grupo de Biofísica Molecular "Sergio Mascarenhas," Instituto de Física de São Carlos, Universidade de São Paulo, São Carlos, São Paulo, Brasil, the §Departamento de Física, Faculdade de Filosofia Ciências e Letras de Ribeirão Preto, Universidade de São Paulo, Ribeirão Preto, São Paulo, Brasil, the ¶Structural Biology Unit, CIC bioGUNE Technological Park of Bizkaia, Derio, Vizcaya, Spain, the ∥IKERBASQUE, Basque Foundation for Science, 48013 Bilbao, Spain, the **Instituto Biofisika, Consejo Superior de Investigaciones Científicas, Universidad del País Vasco/Euskal Herriko Unibertsitatea (CSIC,UPV/EHU), Barrio Sarriena s/n, Leioa, 48940 Bizkaia, Spain, the ‡‡Departamento de Bioquímica, Universidad del País Vasco, Leioa, 48940 Bizkaia, Spain, the §§Departamento de Bioquímica, Instituto de Química, Universidade de São Paulo, São Paulo, São Paulo, Brasil, and the ¶¶Instituto de Biología Molecular y Celular de Rosario (IBR), Rosario, Santa Fe, Argentina*

Edited by Dennis R. Voelker

PlsX plays a central role in the coordination of fatty acid and phospholipid biosynthesis in Gram-positive bacteria. PlsX is a peripheral membrane acyltransferase that catalyzes the conversion of acyl-ACP to acyl-phosphate, which is in turn utilized by the polytopic membrane acyltransferase PlsY on the pathway of bacterial phospholipid biosynthesis. We have recently studied the interaction between PlsX and membrane phospholipids *in vivo* and *in vitro*, and observed that membrane association is necessary for the efficient transfer of acyl-phosphate to PlsY. However, understanding the molecular basis of such a channeling mechanism remains a major challenge. Here, we disentangle the binding and insertion events of the enzyme to the membrane, and the subsequent catalysis. We show that PlsX membrane binding is a process mostly mediated by phospholipid charge, whereas fatty acid saturation and membrane fluidity remarkably influence the membrane insertion step. Strikingly, the PlsX[L254E] mutant, whose biological functionality was severely compromised *in vivo* but remains catalytically active *in vitro*, was able to superficially bind to phospholipid vesicles, nevertheless, it loses the insertion capacity, strongly supporting the importance of membrane insertion in acyl-phosphate delivery. We propose a mechanism in which membrane fluidity governs the insertion of PlsX and thus regulates the biosynthesis of phospholipids in Gram-positive bacteria. This model may be operational in other peripheral membrane proteins with an unprecedented impact in drug discovery/development strategies.

Biological membranes readily adapt in response to various environmental perturbations. Subtle changes in the chemical compositions of acyl chains or head groups of phospholipids can precisely adjust the packing arrangements within the lipid bilayer (1, 2). Altered phospholipid packing properties affect not only the bilayer stability and fluidity, but also the phospholipid-protein interactions and microdomains organization, with a great impact in the physiology of the cells (3). Several external factors, including temperature, pressure, pH, chemicals, ions, radiation, nutrients, and the growth phase of cultured cells, among others, are all capable of modifying the order, packing, and membrane phospholipid composition (1, 4–6).

The most widely distributed pathway for membrane phospholipid formation in bacteria, including important human Gram-positive pathogens such as *Streptococcus pneumonia* and *Staphylococcus aureus*, comprises three enzymes: PlsX, PlsY, and PlsC (7–9) (Fig. 1A). The first step is mediated by PlsX, a phosphotransacylase that catalyzes the conversion of acyl-acyl carrier protein (acyl-ACP)[3] in acyl-phosphate (acyl-PO_4). The second step is catalyzed by the polytopic membrane acyltrans-

[3] The abbreviations used are: acyl-ACP, acyl-acyl carrier protein; DMPC, 1,2-dimiristoyl-*sn*-glycero-phosphatidylcholine; DMPG, 1,2-dimiristoyl-*sn*-glycero-3-phospho-(1'-rac-glycerol); DPPG, 1,2-dipalmitoyl-*sn*-glycero-3-phospho-(1'-rac-glycerol); DOPG 1,2-dioleoyl-*sn*-glycero-3-phospho-(1'-rac-glycerol); POPG, 1-palmitoyl-2-oleoyl-*sn*-glycero-3-phospho-(1'-rac-glycerol); *n*-PCSL, 1-palmitoyl-2-stearoyl(*n*-doxyl)-*sn*-glycero-3-phosphocholine (where *n* = 5 and 14); DPPTC, 1,2-dipalmitoyl-*sn*-glycero-3-phospho(tempo)choline; LPA, lysophosphatidic acid; ESR, electron spin resonance; SPR, surface plasmon resonance; SUV, small unilamellar vesicle; LE, liquid-expanded; LC, liquid-condensed; N, newton; UFA, unsaturated fatty acid; RP2, retinitis pigmentosa 2; BisTris, 2-[bis(2-hydroxyethyl)amino]-2-(hydroxymethyl)propane-1,3-diol; PDB, Protein Data Bank; RU, response unit.
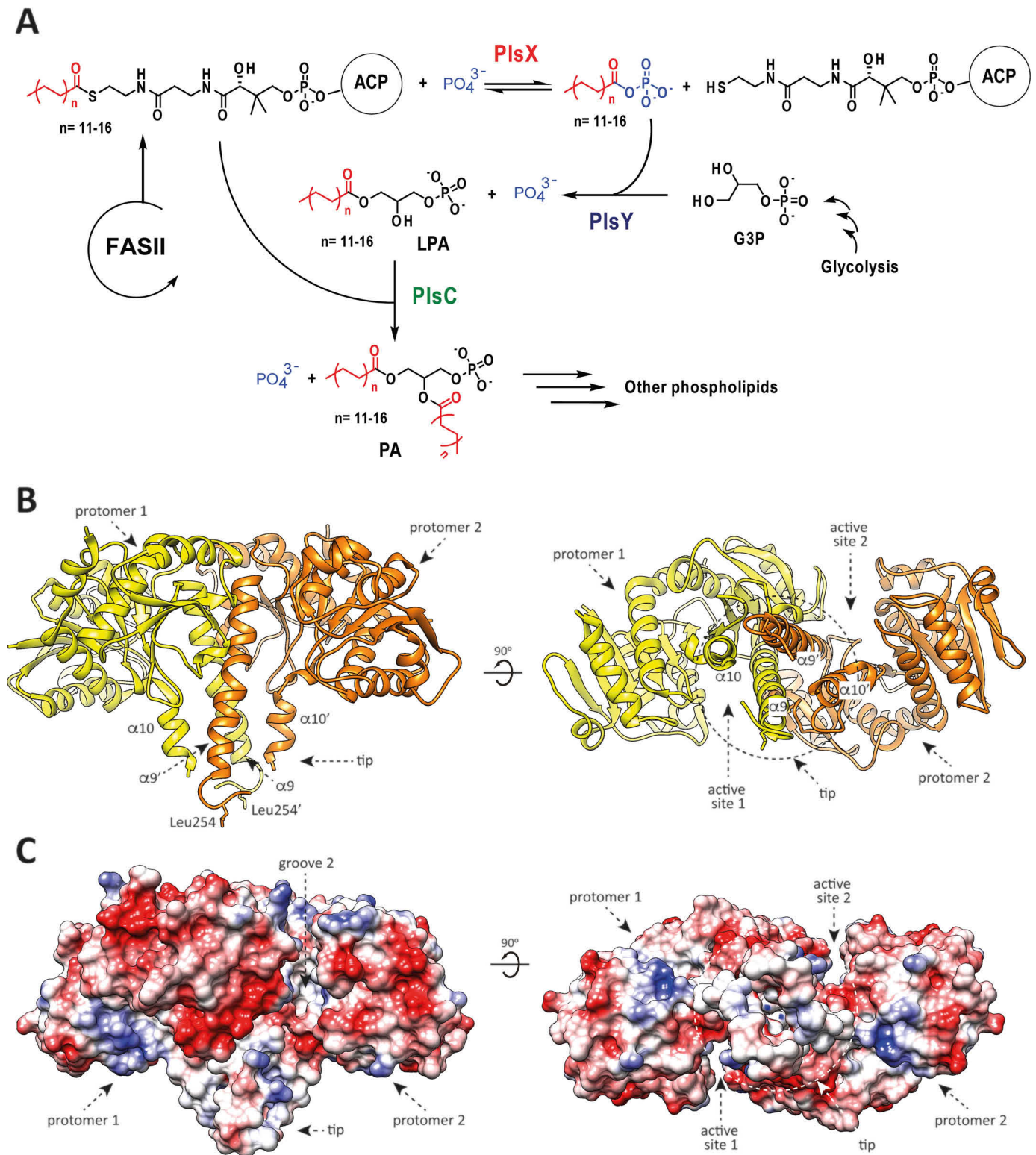
Figure 1. Phospholipid synthesis pathway in Gram-positive bacteria. *A,* this pathway starts with the conversion of a long-chain acyl-ACP end product of fatty acid synthase II (*FASII*) to an acyl-PO$_4$ by PlsX. Then, PlsY transfers the fatty acid from the acyl-PO$_4$ to glycerol 3-phosphate (*G3P*), and finally the LPA is converted to phosphatidic acid (*PA*) by PlsC using acyl-ACP as the acyl donor. *B,* two views showing the cartoon representation of PlsX. The location of (i) the tip, composed of α9, α10, and α9′, α10′ helices, involved in membrane association, and (ii) the proposed active site of each protomer are shown. *C,* two views showing the electrostatic surface representation of PlsX. PlsX is a polar dimeric protein, with hydrophobic and positively charged residues oriented toward the plasma membrane. Negatively charged residues are facing the cytosol. The Poisson-Boltzmann electrostatic color map spans from *red* to *blue*, ranging from −10 to +10 kcal/mol.

ferase PlsY, which transfers an acyl group from acyl-PO$_4$ to position 1 of glycerol 3-phosphate to form 1-acyl-glycerol-3-phosphate or lysophosphatidic acid (LPA). PlsC completes the pathway transferring an acyl group from acyl-ACP to the position 2 of LPA to form 1,2-diacyl-*sn*-glycero-3-phosphate or phosphatidic acid, the universal precursor of phospholipids (7–11). Interestingly, inhibition of the PlsX-mediated reaction results in the shutdown of fatty acid synthesis by FASII. Therefore, PlsX seems to be a key regulatory point that synchronizes FASII with phospholipid biosynthesis (10, 12).

PlsX is a peripheral membrane enzyme homogeneously distributed on the membrane of most bacterial cells, but occasionally exhibiting foci localization (13). To date, two crystal structures of PlsX enzymes have been reported, that of the unliganded forms of PlsX from *Bacillus subtilis* (*Bs*PlsX) (14) and *Enterococcus faecalis* (*Ef*PlsX) (15). Both enzymes crystallized as homodimers with each protomer composed of a Rossmann-fold domain, where the active site is located. Two α-helices form a long hairpin that protrudes away from the main core of each protomer and assemble into a four α-helical bundle subdomain (α9, α10 and α9′, α10′), mediating the formation of an S-shaped dimeric quaternary structure (Fig. 1*B*). The electrostatic surface potential of PlsX revealed a cluster of positively charged residues in the tip of the amphipathic α-helical bundle, interspersed with several hydrophobic residues that form a loop between these helices (14). The α9–α10 loop was proved important to facilitate the direct binding of *B. subtilis* PlsX to the phospholipid bilayer (55). Strikingly, the interaction between PlsX and the bacterial membrane was necessary for phospholipid biosynthesis and viability *in vivo*. However, it was not required for the acyl-ACP:phosphate transacylase enzymatic activity *in vitro* (55). Moreover, PlsX seems to preferentially interact with regions of increased fluidity of *B. subtilis* membranes *in vivo*, suggesting that the membrane composition could play a key influence on PlsX-membrane interaction and regulation of the phospholipid biosynthetic process (16). Here electron spin resonance (ESR), surface plasmon resonance (SPR), and Langmuir films are used to unveil the molecular basis of binding and insertion of PlsX into the membrane.

Results

PlsX preferentially binds to anionic phospholipids

To carefully investigate the binding properties and the impact of membrane fluidity in the binding to PlsX, we regulate the fluidity of phospholipid vesicles by varying three different parameters: (i) fatty acid chain length, (ii) degree of saturation of fatty acids, and (iii) temperature. SPR has proven to be a powerful technique to study protein-ligand and protein-membrane association. Small unilamellar phospholipid vesicles (SUVs) were immobilized on a L1 chip and concentrations of PlsX, ranging from 7.5 nM to 2 μM, were injected and binding affinity constants (K_D) determined (see "Experimental procedures"). PlsX binds to the anionic and saturated 1,2-dimiristoyl-*sn*-glycero-3-phospho-(1′-rac-glycerol) (14:0/14:0; DMPG), but not to the corresponding zwitterionic 1,2-dimiristoyl-*sn*-

glycero-phosphatidylcholine (14:0/14:0; DMPC) (Fig. 2, *A–D*), emphasizing the strict requirement of the negative charge for the protein-phospholipid interaction to occur. We then studied the binding of PlsX to DMPG vesicles above and below the temperature of the gel to liquid-crystalline phase transition (T_m = 24 °C). Interestingly, we clearly observed that the RU intensity reached during PlsX injection on the DMPG surface was higher if the lipid was in the liquid-crystalline fluid phase at 30 °C compared with that observed at 20 °C, which corresponds to the DMPG gel (rigid chain) state (Fig. 2, *A* and *B*) (17). However, we were not able to measure the K_D value for PlsX binding to DMPG SUVs, because equilibrium was not reached during the injection phase. Instead, we determined a 10-fold reduction in the K_D value for PlsX to the phospholipid mixture composed of DMPG and the anionic and unsaturated 1,2-dioleoyl-*sn*-glycero-3-phospho-(1′-rac-glycerol) (18:1/18:1; DOPG; T_m = −18 °C) (3:1 molar ratio) at 20 °C (1.13 μM) relative to that observed at 30 °C (95 nM; Fig. 2). In contrast, a similar K_D value, in the low nanomolar range, was observed for the anionic and saturated 1,2-dipalmitoyl-*sn*-glycero-3-phospho-(1′-rac-glycerol) (16:0/16:0; DPPG; T_m = 41 °C) at 20 (94 nM) and 30 °C (115 nM), both in the gel phase (Fig. 2). Taken together, our SPR experimental data indicate that PlsX exhibits high specific binding properties to phospholipids, in terms of charge and degree of unsaturation of fatty acids components of the phospholipid bilayer, however, a clear correlation between fluidity and PlsX binding was not observed.

Membrane fluidity facilitates the insertion of PlsX into anionic phospholipid monolayers

To evaluate whether membrane fluidity is a major factor that influences PlsX insertion, we analyzed the insertion of PlsX into phospholipid membranes employing Langmuir films at various initial pressure (π0) values. A series of phospholipid monolayers were prepared bearing the same polar head group, phosphatidylglycerol, but carrying different fatty acid chain lengths and degrees of unsaturation. PlsX was injected underneath a lipid monolayer prepared at the air-water interface, and the interaction of PlsX to the monolayer was quantified by surface pressure measurements. There are, in monolayers, analogous states to the liquid-crystal (fluid chain) and gel (rigid chain) states of the phospholipid bilayer, which are termed the liquid-expanded (LE) and liquid-condensed (LC) states, respectively (18). The critical pressure of insertion (πc), determined by the abscissa intercept of the surface pressure increase *versus* π0 plot, indicates the protein propensity for membrane insertion. Hence, larger πc indicates a higher propensity for protein insertion into monolayers. Strikingly, the largest value of πc (33 mN/m) was observed for PlsX with saturated DMPG at the LE state (30 °C; Fig. 3*A*), being a value within the range of 30–35 mN/m, which was estimated as the lateral pressure of biomembranes (19–21). The degree of PlsX insertion into monolayers was clearly smaller in the LC state of DMPG (20 °C) and DPPG (30 °C), as judged by πc ~ 29 mN/m, indicating that the insertion of PlsX directly correlates with membrane fluidity. Moreover, addition of PlsX into monolayers comprised of DOPG:DMPG at 1:3 and 3:1 molar ratios, and pure DOPG resulted in a marked decrease in the critical surface pressure (πc of 31.6,
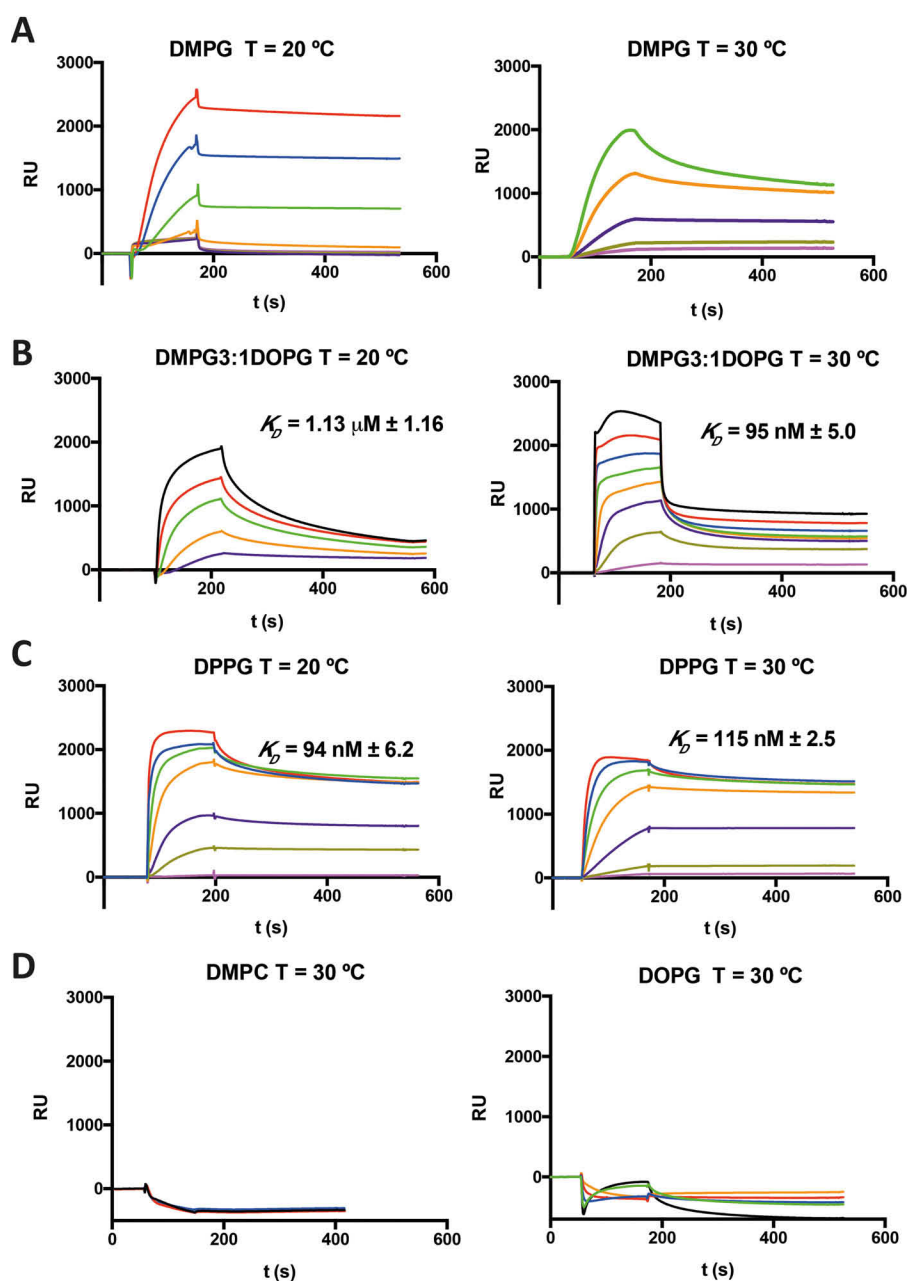
Figure 2. Analysis of PlsX binding to phospholipid vesicles with different fluidity by SPR. SPR sensograms of PlsX association with (*A*) DMPG, (*B*) DMPG:DOPG (3:1) (mol/mol), (*C*) DPPG, and (*D*) DMPC and DOPG SUVs. Sensograms were obtained by a concentration series of PlsX: *black line,* 2 μM; *red line,* 1 μM; *blue line,* 0.5 μM; *light green line,* 0.25 μM; *orange line,* 0.12 μM; *purple line,* 0.061 μM; *dark green line,* 0.030 μM; *magenta line,* 0.015 μM; *grey line,* 0.007 μM. The K_D was calculated by using a general steady-state equilibrium model.

29.7, and 29.5 mN/m, respectively) as compared with pure DMPG in the LE state.

In addition to the measurement of the critical pressure, the synergy factor (*a*), defined as the slope +1 of the curves of $\Delta\pi$ *versus* π0 (Fig. 3*A*), is an additional parameter used to determine the selective adsorption between peripheral membrane proteins and phospholipids using the monolayer model (22, 23). A value of *a* > 0 was obtained for all phospholipids analyzed, corresponding to favorable conditions for PlsX-monolayer binding (Fig. 3*B*). Interestingly, even though the unsaturated DOPG is in the LE state (*a* = 0.22 ± 0.04), the saturated DMPG in the LE state clearly favors PlsX insertion into the phospholipid monolayer (*a* = 0.4 ± 0.03), which is consistent

with the corresponding πc values. Therefore, the insertion of PlsX into phospholipid monolayers seems to be modulated not only by the physical state of the phospholipids, but also by the degree of unsaturation. Altogether, the experimental data demonstrate that the insertion of PlsX into membranes is highly favored by saturated phospholipids in the LE state (fluid phase) than by unsaturated phospholipids or phospholipids in the LC state (gel phase; Fig. 3).

PlsX insertion modifies the dynamics of anionic phospholipid bilayers

To investigate the effects of protein insertion on the structural dynamics of phospholipid bilayer membranes, we applied
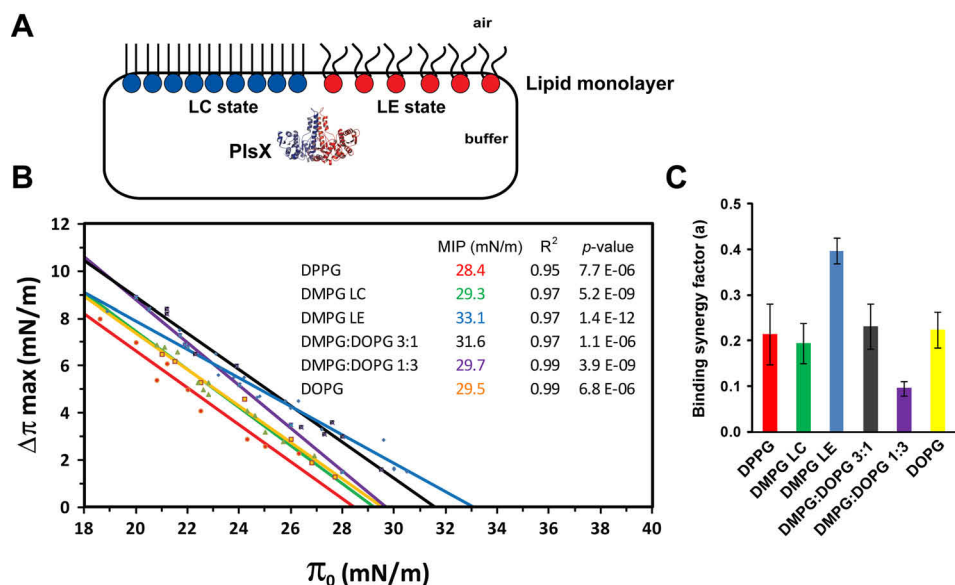
Figure 3. Determination of the critical surface pressure (π_C) and synergy factor of PlsX WT enzyme in the presence of different phospholipids. *A*, schematic representation of the Langmuir films experiments to study the interaction between PlsX protein and phospholipid monolayers on liquid-condensed and liquid expanded states. *B*, surface pressure increase ($\Delta\pi$) was plotted as a function of the initial surface pressure (π_0) to determine the critical pressure of PlsX with DMPG in the LE and LC states and DPPG (LC), DOPG (LE), and DMPG:DOPG (1:1 and 3:1) (LE) monolayers by extrapolating the curve to the *x* axis. *Inset*, at least seven data points were used to generate statistical significant linear regression to obtain the maximum insertion pressure (*MIP*) or π_C values for each condition. *C*, synergy factor of PlsX WT in the same phospholipid monolayers described in *A*. The subphase contained 25 mM HEPES, pH 7.4, and 300 mM NaCl. The final concentration of PlsX was 100 nM.

spin labeling ESR spectroscopy. Spin labeling ESR is a powerful spectroscopic tool to study protein-lipid interactions from both protein and lipid perspectives (24–26). Here we used nitroxide spin probes attached (i) to the polar head group region of 1,2-dipalmitoyl-*sn*-glycero-3-phospho(tempo)choline (DPPTC), to monitor protein-induced changes in the lipid/water interface, or (ii) to carbons 5 or 14 of the lipid acyl chain of 1-palmitoyl-2-stearoyl(*n*-doxyl)-*sn*-glycero-3-phosphocholine (*n*-PCSL, where n = 5 and 14; 5-PCSL and 14-PCSL, respectively), to monitor protein-induced changes in the hydrophobic core of the phospholipid bilayer (26).

Fig. 4*A* illustrates representative ESR spectra of the spin-labeled lipids DPPTC, 5-PCSL, and 14-PCSL embedded in DMPG SUVs in the absence and presence of 2 mol % of PlsX. Addition of the protein to the SUVs promoted spectral changes for all spin probes, indicating that the protein perturbs the DMPG membranes from its surface down to the center of the bilayer. Strikingly, the most pronounced effects were observed in the fluid phase (Fig. S1*A* and Fig. 4*A*). The parameters h_{+1}/h_0, the ratio between the height of the low (h_{+1}) and the central (h_0) field resonance lines of the DPPTC and 14-PCSL ESR spectra, and $2A_{max}$, the outer hyperfine splitting of the 5-PCSL ESR spectrum (Fig. 4*A*), are useful parameters defined on the spectra very sensitive to the probes rotational mobility (27). The larger the h_{+1}/h_0 or the lower the $2A_{max}$, the less ordered or more dynamic are the spin probes. PlsX binding to the surface of DMPG SUVs decreases h_{+1}/h_0 of DPPTC and 14-PCSL and increases $2A_{max}$ of 5-PCSL (Fig. 4*A*). This result indicates that PlsX induces a molecular ordering effect and/or a reduction of the lipid mobility that extends from the membrane surface all the way down to the phospholipid bilayer center. To further confirm these results, we performed nonlinear least-squares simulations of the ESR spectra obtained at 30 °C, which showed

that both the rotational diffusion rate (R) and order parameter (S_0) are altered by the enzyme. PlsX decreased the phospholipid mobility by 15% (6.61 to 5.62 × 10^7 s^{-1}) for DPPTC, 18% (1.35 to 1.10 × 10^8 s^{-1}) for 5-PCSL, and 29% (3.02 to 2.14 × 10^8 s^{-1}) for 14-PCSL. Significant changes were also observed in the order parameter ΔS_0 of 0.14 for DPPTC, 0.08 for 5-PCSL, and 0.06 for 14-PCSL.

We also investigated the influence of the protein on the structural dynamics of DMPC (Fig. 1*C*), DPPG, 1-palmitoyl-2-oleoyl-*sn*-glycero-3-phospho-(1′-rac-glycerol) (POPG), and on an equimolar mixture of DMPG/POPG. Fig. 4, *B* and *C,* show the h_{+1}/h_0 and $2A_{max}$ parameters for DPPTC and 5-PCSL, respectively, as a function of the membrane fluidity, as determined by $2A_{max}$ (27). It is evident that not only the negative charge is important for the protein-induced perturbations, but also the degree of unsaturation of fatty acids. Interestingly, the ordering and reduced mobility effect promoted by PlsX is higher for DPPG in the gel phase (30 °C) than for POPG in the fluid phase (30 °C). Addition of 50% DMPG to POPG increases the effect of the protein by 1.6-fold for DPPTC and 2-fold for 5-PCSL. SUVs of DMPG, DMPG:POPG (1:1), and POPG at 30 °C have similar fluidity (Fig. 4*B*), however, the PlsX effect was drastically reduced by the presence of unsaturations in the vesicles (Fig. 4*C*). This enables discrimination of the influence of unsaturations and membrane fluidity on PlsX-phospholipid insertion.

Differential insertion of PlsX and PlsX[L254E] mutant into phospholipids

With the aim to disentangle the binding and insertion events of PlsX to the membrane, and the subsequent acyl-phosphate transfer to the membrane, we employed the PlsX[L254E] mutant. PlsX[L254E] contains a single-point mutation in the $\alpha9-\alpha10$ loop
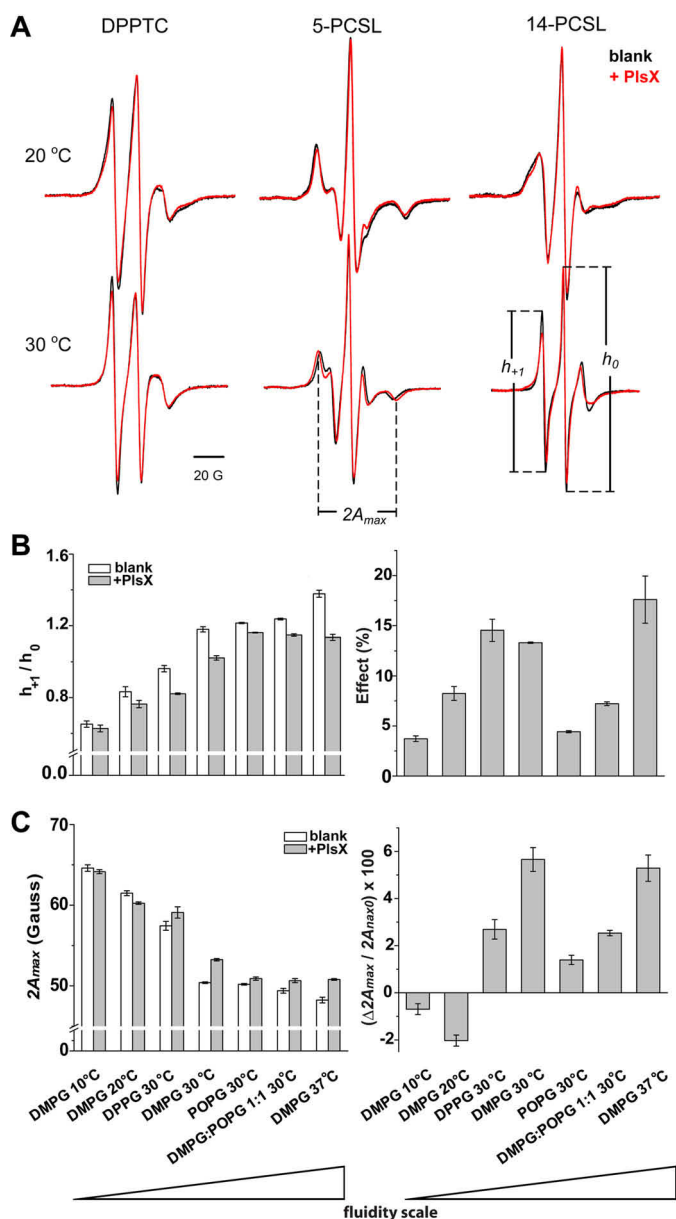
Figure 4. Effects of PlsX on the ordering and mobility of the lipids monitored by ESR spectroscopy. *A*, ESR spectra of DPPTC, 5-PCSL, and 14-PCSL in DMPG SUVs in the absence (*black*) and presence (*red*) of PlsX at 1:47 protein-to-lipid molar ratio obtained at 20 and 30 °C. The parameters h_{+1}/h_0 and $2A_{max}$ are defined as illustrated in the spectra. *B* and *C*, show the changes on (*B*) h_{+1}/h_0 of DPPTC and (*C*) $2A_{max}$ of 5-PCSL promoted by 2 mol % of PlsX on the *left panel* and the percentage of those changes on the *right panel* as a function of increasing membrane fluidity. The fluidity scale was qualitatively determined by $2A_{max}$. Each *error bar* represents the mean of two independent determinations.

(Fig. 1*B*) that severely affects membrane association *in vivo* and also compromises lipid interaction *in vitro* (55). Although the active site remained intact and PlsX[L254E] is catalytically active *in vitro*, the protein cannot support phospholipid synthesis *in vivo*, strongly supporting the notion that proper membrane association is necessary for transfer of product to PlsY, the next enzyme in the pathway (55). Here, we carefully measured the binding properties of PlsX[L254E] to SUVs by SPR. PlsX[L254E] displays the same binding preference for anionic and saturated lipids as the WT protein (Fig. 5*A*), as reflected by a 2-fold reduc-

tion in the binding affinity of PlsX[L254E] for DMPG:DOPG (3:1) compared with WT PlsX. We then investigated the impact of DMPG SUVs to the structure of PlsX and PlsX[L254E], by thermal unfolding experiments followed by CD in the far-UV region. It is worth noting that the far-CD spectrum of PlsX[L254E] superimpose very well with that of the WT enzyme, indicating that both proteins are properly folded (Fig. S2*A*). The cooperativity of PlsX and PlsX[L254E] unfolding revealed a two-state reaction in the absence of anionic phospholipids (Fig. S2*B*). This cooperativity is lost for PlsX in the presence of DMPG SUVs. Interestingly, the addition of DMPG SUVs to PlsX[L254E] induced a different unfolding pathway, indicating that the structural modification of the hydrophobic loop between helices α9 and α10 severely affected the mechanism of interaction of PlsX with phospholipids.

We then studied the impact of the single-point mutation on PlsX-phospholipid insertion by Langmuir film assays. We compared the insertion of PlsX with that of the PlsX[L254E] mutant into DMPG monolayers in the LC and LE states prepared at various initial pressure (π0) values (Fig. 5*B*). As depicted in Fig. 5*B*, the lower πc value obtained for the PlsX[L254E] mutant (30.8 mN m^{-1}) in the presence of the DMPG LE state, compared with that obtained for the WT enzyme (33.1 mN m^{-1}) clearly indicates that PlsX[L254E] binds but does not insert into fluid phospholipid membranes. Interestingly, the synergy factor values (Fig. 5*C*) were in agreement with the πc values shown in Fig. 5*B*, confirming the insertion of PlsX into DMPG in LE state and no insertion of PlsX[L254E]. Finally, ESR was used to investigate the effects of the PlsX[L254E] mutant on the structural dynamics of DMPG lipid bilayers in the liquid-crystalline (fluid chain) and gel (rigid chain) phases. Interestingly, PlsX[L254E] promoted minimal spectral changes only at the polar head group region, indicating that the mutant could only attach superficially to the membrane (Fig. 6 and Fig. S1*B*). Furthermore, the effects of the mutant on the ordering and dynamics of the DPPTC were only observed in the DMPG gel phase, as shown by the DPPTC spectrum at 10 °C. This result shows that the weak protein binding to the DMPG surface does not change the rotational diffusion rates and the order parameter of the lipid head group in the fluid phase.

To further explore the differences between the PlsX and PlsX[L254E] mutant lipid insertion ability, we decided to analyze the insertion of both enzymes using membrane lipids isolated from *B. subtilis* cells grown at 37 °C and also after a cold-shock (from 37 to 20 °C) to induce changes in the length, branched chains, and Δ5-monounsaturated glycerol phospholipid percentages (28). First, we analyzed the thermal melting profiles of total lipids extracted from *B. subtilis* by DSC assays. We confirmed that liposomes prepared from lipids extracted at 20 °C display a lower melting temperature compared with those containing lipids extracted at 37 °C (Fig. S3). This indicates a different lipid composition suggestive of higher content of unsaturated fatty acid (UFAs) and anteiso-branched chain fatty acids, both "fluidizing lipids" as previously described (28, 29). Then, we determined the insertion of PlsX and the PlsX[L254E] mutant into small unilamellar vesicles made of lipids extracted from *B. subtilis* by ESR assays. Interestingly, 5-PCSL ESR spectra in the absence and presence of PlsX and PlsX[L254E] using
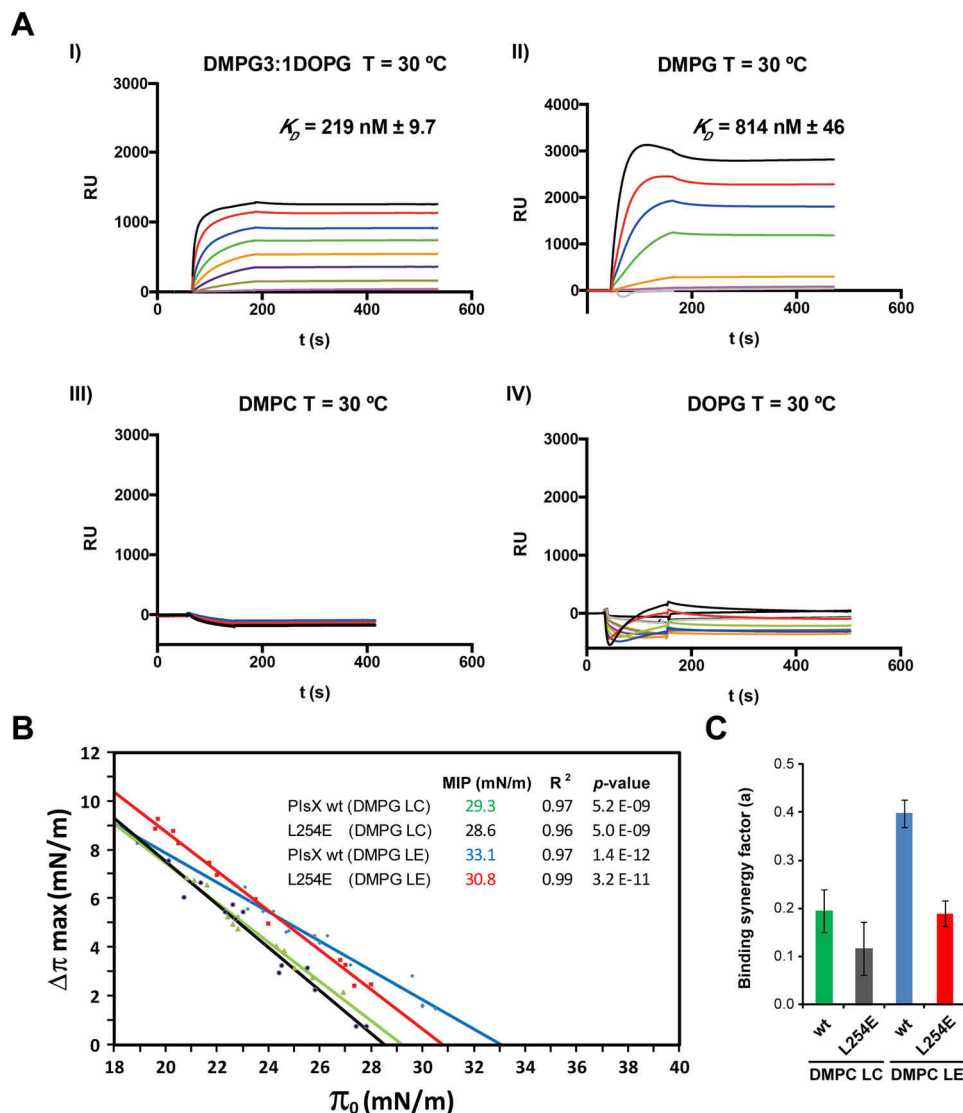
Figure 5. Analysis of PlsX^L254E binding and insertion to phospholipids with different fluidity by SPR and Langmuir films assays. *A,* SPR sensograms of PlsX^L254E association with (*I*) DMPG:DOPG (3:1), (*II*) DMPG, (*III*) DMPC, and (*IV*) DOPG SUVS at 30 °C. Sensograms were obtained by concentration series of PlsX: *black line,* 2 µM; *red line,* 1 µM; *blue line,* 0.5 µM; *light green line,* 0.25 µM; *orange line,* 0.12 µM; *purple line,* 0.061 µM; *dark green line,* 0.030 µM, *magenta line,* 0.015 µM, *grey line,* 0.007 µM. The K_D was calculated by using a general steady-state equilibrium model. *B,* determination of the critical surface pressure (π_c) of the PlsX^L254E mutant compared with the WT enzyme in the presence of DMPG phospholipid monolayers at LC and LE states. Surface pressure increase ($\Delta\pi$) was plotted as a function of the initial surface pressure ($\pi0$) to determine the critical pressure of PlsX WT and PlsX^L254E mutant in the LE and LC states monolayers by extrapolating the curve to the *x* axis. *Inset*: at least nine data points were used to generate statistical significant linear regression to obtain the maximum insertion pressure (*MIP*) or π_c values for each condition. *C,* synergy factor of PlsX^L254E and WT in DMPG (LC) and DMPG (LE) monolayers. The subphase contained 25 mM HEPES, pH 7.4, and 300 mM NaCl. The final concentration of PlsX was 100 nM.

lipids from cells grown at 37 °C (Fig. S3) showed close agreement with those obtained with pure DMPG (Figs. 4*A* and 6). Interestingly, we also detected spectral differences in the presence of PlsX, between vesicles obtained with *B. subtilis* lipids extracted from cells grown at 37 °C from those obtained from cells grown after a cold shock treatment. Specifically, we have observed a higher effect of PlsX, represented by the order parameter *Szz* values (30), with lipids extracted at 37 °C (Fig. S3), which is in accordance with our data using UFAs Δ9 (POPG 30 °C, in Fig. 4). Moreover, we have also performed monolayer assays with the PlsX and PlsX^L254E mutant using *B. subtilis* lipids extracted at 37 °C (Fig. S3), and the results were in the same line compared with those reported using DMPG monolayers (Fig. 5*b*). Altogether, we conclude that PlsX^L254E

displays a significant reduction in its ability to insert into lipid monolayers and bilayers, thus preventing the mutant protein to be anchored in the *B. subtilis* membrane. This supports the hypothesis that the channeling function of PlsX requires its proper insertion into the membrane (55).

Discussion

Peripheral membrane enzymes play critical roles in many biological functions such as membrane trafficking, membrane biosynthesis, and remodeling and cell signaling (31). Peripheral membrane enzymes attach temporarily to one face of the lipid bilayer or to other membrane proteins (1). They interact weakly with the membrane mainly by noncovalent interactions including electrostatic and hydrogen bonds (32). The dissociation rate
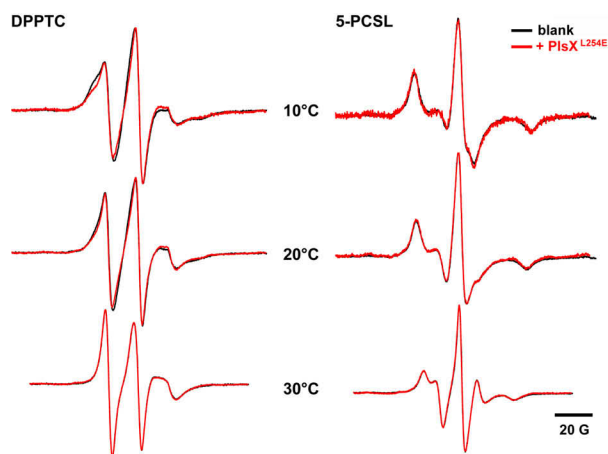
Figure 6. Line shape ESR spectral changes promoted by the PlsX[L254E] **mutant.** ESR spectra of DPPTC (*left*) and 5-PCSL (*right*) in anionic DMPG SUVs at different temperatures (10, 20, and 30 °C) without (*black*) and with L254E mutant (*red*) at 1:47 protein-to-lipid molar ratio.

constants of many peripheral membrane enzymes remain unknown, making their unambiguous classification and the understanding of the association mechanism difficult. The determination of the protein subcellular localization became, in most of the cases, the sole criteria to discriminate between integral or peripheral membrane enzymes. A deep understanding of the physical properties of biological membranes and their influence on the molecular mechanisms by which enzymes interact with substrates and mediate catalysis remain a major challenge.

Amphipathic α-helices represent a common motif that mediate the interaction of peripheral enzymes to the membrane. They bind to lipid membranes by a physical adsorption mechanism in which electrostatic and hydrogen bond interactions are dominant (33). This process commonly follows three steps: (i) the binding is initiated by the electrostatic attraction of the positively charged peptide to the negatively charged membrane head group; (ii) the peptide is then disposed into the plane of binding where its exact position depends on the hydrophobic/hydrophilic balance of the molecular groups and forces involved; and (iii) the bound peptide changes its conformation. In certain cases, peptides can acquire or modify their secondary structure when associated with the membrane (34, 35). We previously identified a loop rich in hydrophobic residues (254–263) localized at the tip of PlsX, which plays a critical role in mediating protein-membrane interaction. This loop is part of a conserved α-helical hairpin, comprising the amphipathic helices (i) α9 (residues 232–249), (ii) the hydrophobic loop (residues 254–263), and (iii) α10 (residues 264–276), also involved in the dimerization mechanism of PlsX (Fig. 1*B*), typical structural features of peripheral membrane proteins. Recently, Jiang *et al.* (36) reported a new PlsX crystal structure from *B. subtilis* in which in one protomer, the hydrophobic loop, is able to fold into a short amphipathic α-helix in the presence of detergent.

Interestingly, whereas the interaction between PlsX and membrane phospholipids was necessary for normal phospholipid synthesis and viability *in vivo*, it was not required for the acyl-ACP:phosphate transacylase enzymatic activity *in vitro* (55). Therefore, we propose a model in which proper mem-

brane interaction *in vivo* is required for the appropriate delivery of acyl-phosphate, the product of the PlsX-mediated reaction, to its protein partner PlsY (see Ref. 55). We now determined the binding constant and insertion of PlsX in the presence of lipid vesicles and monolayers of saturated and unsaturated phospholipids with different fluidity. We calculated the perturbation effects and synergy factor to analyze the membrane insertion capacity of PlsX toward phospholipids of different nature. Strikingly, we determined that membrane fluidity adjusts the insertion and activity of PlsX in the membrane. Because the activity, channeling, of PlsX depends on membrane insertion, fluidity might be a way to regulate phospholipid biosynthesis in Gram-positive bacteria (Fig. 7). These results markedly contribute to understand how catalytic efficiencies can be modulated by membrane composition or protein mobility.

The calculated electrostatic surface potential of PlsX from *B. subtilis* shows a region containing several positively charged residues located perpendicular to the main groove of the enzyme (Fig. S4). This patch is conserved among other PlsX homologues (Fig. S5). Interestingly, the crystal structures of different enzymes in complex with ACP support a preferred binding orientation of the acidic carrier ACP with respect to the surface of the protein partner (Fig. S6) (37–42). This overall orientation is in agreement with the proposed ACP chain-flipping mechanism in which the acyl-chain carried inside ACP can partition from the hydrophobic ACP pocket into the hydrophobic active-site pocket of the enzyme (43). Therefore, we hypothesize the acidic acyl-ACP donor binds on the surface-exposed positive patch of PlsX, with the hydrophobic acyl-containing channel oriented along with the main groove. To test this hypothesis, we performed docking calculations to investigate the interaction between (i) PlsX and ACP from *B. subtilis* and (ii) PlsX with 4′-phosphopantetheine myristate (Fig. S7) (14, 44). Remarkably, both calculations agreed well with our hypothesis. First, the top hits show that ACP interact with the surface-exposed positive patch of PlsX, with Ser-37, which is *O*-pantetheine 4′-phosphoryl modified, oriented toward the groove (Fig. S7). Second, the 4′-phosphopantetheine myristate lies inside the groove with the phosphoric group heading toward the ACP-binding site (Fig. S7). The ACP-binding surface identified in PlsX is on the opposite side of the tip, an orientation that is compatible with PlsX accessing acyl-ACP from the cytoplasm, as expected. Because PlsX is clearly membrane associated in cells, transfer of acyl chains from acyl-ACP to PlsX must involve predominantly the diffusion of cytoplasmic acyl-ACP to the membrane and not vice versa. Our model also highlights that the active site of PlsX is relatively far from the bilayer where the acyl chains must become inserted after transacylation. Transfer of acyl-phosphate may thus involve deeper insertion of PlsX into the membrane (Fig. 7 and Fig. S5).

We also observed that lipid unsaturation has a negative effect in PlsX association with the membrane. We suppose that the significant repulsion effect generated by the unsaturated lipids could be due to a physical issue because, in our assays, these phospholipids contain one double bond in the fatty acid chain that would possibly prevent membrane insertion of PlsX. Although information on the selective insertion of peripheral proteins to membrane lipids is still largely lacking, the occur-
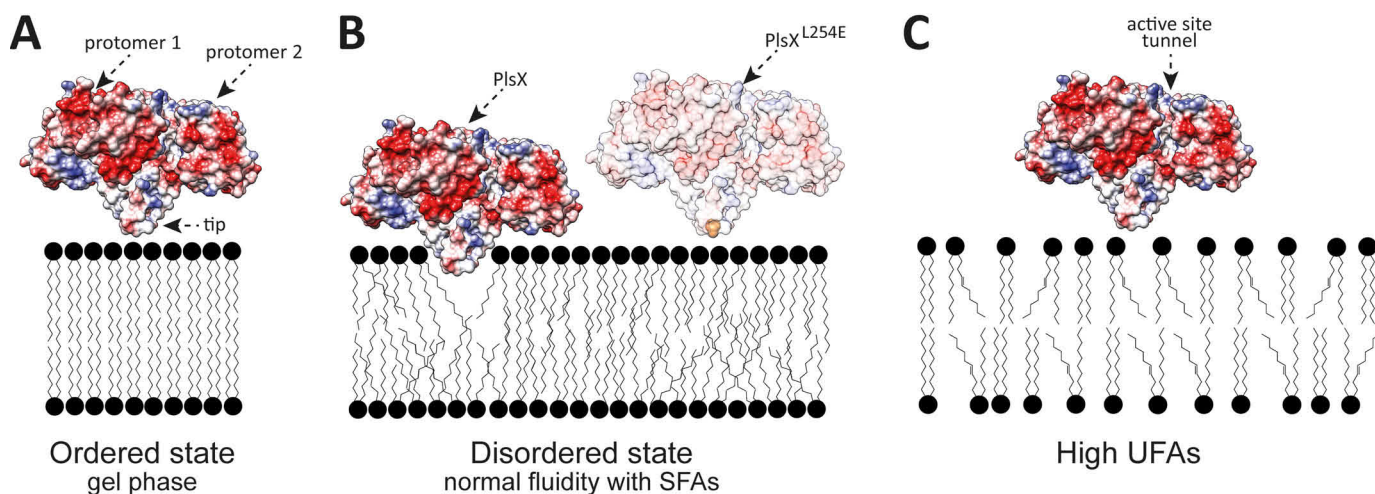
Figure 7. Models of binding and insertion of acyltransferase PlsX into membrane phospholipids. Dependence of membrane fluidity and lipid physical states on binding and insertion of PlsX (*A*) ordered state, (*B*) disordered state, and (*C*) high content of UFAs.

rence of this repulsion effect has been suggested in two peripheral membrane proteins, the human photoreceptors retinitis pigmentosa 2 (RP2) and recoverin (22). RP2 showed high specificity for saturated phospholipids (known to be located in microdomains) and repulsion to unsaturated fatty acids. In contrast, recoverin showed the opposite, *i.e.* higher specificity for polyunsaturated phospholipids than for saturated phospholipids, as expected due to more than 60% of the fatty acid components of the photoreceptor membranes are polyunsaturated. On the other hand, the phospholipids of *B. subtilis* membranes have negligible amounts of UFAs (around 2%) in normal conditions. Nevertheless, the total amount of UFAs can be increased 4–5 times via an acyl-lipid desaturase (Δ5-Des), which is induced after a temperature downshift to regulate the membrane cell fluidity (28, 29, 45). This desaturation reaction is a post-biosynthetic modification of the phospholipid acyl chain that does not require *de novo* synthesis of glycerophospholipids. Therefore, the repulsion effect of PlsX for phospholipids containing UFAs might be part of a mechanism to down-regulate the total phospholipid synthesis observed at low growth temperature in *B. subtilis*.

An interesting question that remained unresolved is the true meaning of the PlsX foci that have been recently reported (13). Our experimental data suggest that PlsX is mostly homogenously distributed into the bacterial cell membrane *in vivo*. Strikingly, PlsX foci were transiently redistributed in this uniform pattern. The transitory nature suggests that they could represent physiological oligomeric states related to the regulation of PlsX activity. However, foci are unlikely to reflect the storage of inactive or surplus enzymes, because there was no correlation between the appearance of foci and the overexpression levels of the enzyme. PlsX, as well as other peripheral membrane proteins, preferentially interact with regions of increased fluidity in *B. subtilis* cells (16, 36). In addition, peripheral membrane proteins form clusters of proteins in the form of "transient oligomers" when interacting with the lipid bilayer and this phenomenon is intensified with an increase in protein radius and depth of penetration into the hydrophobic region of the membrane (46). Based on these evidences, we interpret that

PlsX foci observed *in vivo* might correspond to regions with higher fluidity in the cytoplasmic membranes of *B. subtilis* (13, 16, 36, 47). We propose PlsX preferably inserts deeper into more fluid, but with null or low unsaturated fatty acid content, giving rise to the nonspecific and transitory formation of oligomers in the form of foci at the membrane.

Experimental procedures

Bacterial strains, plasmid construction, and growth conditions

The *plsX* gene from genomic DNA of *B. subtilis* PY79 was amplified by PCR using Phusion DNA polymerase (New England Biolabs), using the following oligonucleotides: NdeI-PlsX-F, 5′-GCACATATGAGAATAGCTGTAGATG-3′ and XhoI-PlsX-R-nonstop, 5′-GTAGGATCCCTCGAGGTACT-CATCTGTTTTTTC-3′, and inserted into pET24b (T7 promotor) within NdeI and XhoI sites to generate pET24b-*plsX*, which expressed *Bs*PlsX with a C-terminal His₆ tag in *Escherichia coli* BL21(DE3). Site-directed mutant PlsX^L254E^ was performed employing a Phusion Site-directed Mutagenesis Kit (Thermo Fisher Scientific), using the following oligonucleotides: PlsX-L254E-F, 5′-CGTAATGACGTCTACTGAGACA-TCCAAGCTTGCAG-3′ and PlsX-L254E-R, 5′-CTGCAAGC-TTGGATGTCTCAGTAGACGTCATTACG-3. In general, *E. coli* was grown in Luria-Bertani broth medium or on plates at 37 °C with aeration containing 50 μg ml^{-1} kanamycin.

Expression and purification of BsPlsX

Plasmids pET24b-*plsX* and those carrying the corresponding *plsX* mutants were used to transform *E. coli* BL21(DE3)-competent cells for protein expression. *Bs*PlsX WT and mutants were induced at OD$_{600}$ 0.6 – 0.8 with 0.8 mM isopropyl 1-thio-β-D-galactopyranoside during 16 h at 18 °C. Cells were collected by centrifugation (6000 rpm, 4 °C, 15 min), and cell pellets were lysed with a sonicator. Soluble proteins were applied to a Ni^{2+}-agarose column and washed with 25 mM HEPES, pH 7.4, 300 mM NaCl (buffer A), and 50 mM imidazole. His-tagged proteins were eluted with buffer A containing 300 mM imidazole. Purified proteins were applied to a calibrated Superdex 200 (GE Healthcare) gel filtration column and eluted with buffer A

without imidazole. The resulting PlsX and mutants preparation displayed a single protein band (Fig. S8) when run on a 12% NuPAGE BisTris precast gel stained with SimplyBlue SafeStain (Invitrogen). The purified dimeric recombinant PlsX and mutants were stored at −80 °C in buffer A.

Lipid vesicles preparation

The phospholipids DMPC, DMPG, DPPG, DOPG, and POPG (Fig. S9), and the spin labels *n*-PCSL (where *n* = 5 and 14), and DPPTC were purchased from Avanti Polar Lipids, Inc. (Alabaster, AL) and used without further purification. Lipid vesicles were prepared as follows: aliquots of lipid stock solutions in chloroform/methanol, 1:1 (v/v), were added into a glass tube, dried under a N_2 flow, and centrifuged under vacuum for 5 h to remove traces of organic solvent. The resulting lipid film was hydrated in buffer A at a temperature above the main phase transition of the lipid for 2 h and submitted to six freeze-thaw cycles. SUV were obtained by subjecting phospholipid suspension to bath sonication until a clear solution was obtained, indicating the formation of unilamellar vesicles. The size of SUVs was determined by dynamic light scattering measurements using a ZetaSizer Nano-S (Malvern). It is worth mentioning that the convenient phase transition temperature of the 14:0 DMPG (T_m = 23 °C) allowed performing the binding/insertion experiments both in the fluid phase and gel phase of the membrane, without compromising PlsX structure (T_m = 55 °C). The very high phase transition temperatures of 16:0 DPPG (41 °C) and 18:0 DSPG (55 °C) precluded working with PlsX in the fluid phase of the membranes, due to protein denaturation/unfolding for temperatures higher than the lipids T_m.

SPR experiments

SPR experiments were performed at 20 and 30 °C in 10 mM HEPES, pH 7.5, and 300 mM NaCl (HBS buffer) using a BIAcore 3000 system (GE Healthcare). The chip surfaces were previously washed with 0.05 M NaOH:isopropyl alcohol (2:3) and 20 mM CHAPS. 1 mM DMPG, DPPG, DMPG:DOPG (2:1), DOPG, and DMPC SUVs prepared in HBS were immobilized on the sample channel of a L1 chip at a density of 3000 RU (10 μl at a flow rate of 5 μl/min). 10 μl of BSA (1 mg/ml) was injected at a flow rate of 5 μl/min on the reference channel of the same chip. PlsX and PlsX[L254E] in HBS were injected at a flow rate of 30 μl/min for 1–2 min. SUVs were washed with 0.05 M NaOH: isopropyl alcohol (2:3) and 20 mM CHAPS between sample injections. Concentration series of PlsX and PlsX[L254E] (from 2 μM to 7.5 nM) were injected and affinity constants (K_D) were calculated using a general steady-state equilibrium model.

Circular dichroism analysis

CD experiments were performed in a J-720 (JASCO Corp., Tokio, Japan) spectropolarimeter using 0.1-cm light path Hellma 110-QS quartz cuvette analyzing a 5 μM protein solution in 10 mM buffer phosphate, pH 7.5, with 300 mM sodium fluoride at 20 °C. Far-UV measurements were performed over a range of 280 to 195 nm at 100 nm/min collecting data at each 1 nm at 20 °C. Data presented constitute an average of 10 consecutive measures through the sample. Thermal dependences of the ellipticity were monitored in a range from 20 to 90 °C at 222

nm, in the absence or presence of lipid vesicles (ratio L/P 50), using a Peltier thermal device. Temperature was increased stepwise by 1°/min. The experiments were performed in duplicate.

Monolayer studies (Langmuir films)

Protein-phospholipid interactions were studied with the Langmuir film balance technique using a Kibron microtensiometer (μTROUGH SX, Kibron Inc., Helsinki, Finland). The aqueous subphase (buffer A: 25 mM HEPES, pH 7.4, and 300 mM NaCl) allows the formation of a compressible monolayer with the polar head group oriented toward water. All experiments were carried out in a controlled atmosphere at 20 or 30 °C. Monomolecular films of the indicated lipid were spread on buffer B subphases (volume of 1250 μl) from chloroform. After spreading the film, 5 min was allowed for solvent evaporation. The protein was injected in the aqueous subphase with a 10-μl Hamilton syringe, and pressure increases were continuously recorded as a function of time. The data were analyzed with the FilmWareX 3.57 program (Kibron Inc.). When injected into buffer B (*i.e.* in absence of lipid monolayer), the protein induced a superficial tension of 18.5 mM/m. Measurements were performed at temperatures above (30 °C) and below (20 °C) the phase transition temperature for DMPG, at 20 and 30 °C (gel phase) for DPPG, 20 and 30 °C (fluid phase) for DOPG and DMPG/DOPG mixture, and 30 °C (fluid phase) for *B. subtilis* lipids.

ESR assays

Continuous wave ESR measurements were performed on a Varian E-109 X-band (9.5 GHz) spectrometer. SUVs containing the appropriate nitroxide-labeled lipids were prepared the same way as unlabeled vesicles. Protein was added to preformed unilamellar vesicles at the desired concentrations. Protein-free and protein-containing SUV samples were transferred to 1.5-mm diameter glass capillaries and centrifuged at 10,000 rpm for 10 min to increase the signal-to-noise ratio. The capillaries were set into a quartz tube containing a mineral oil bath, which helps to keep the sample temperature stable. The thermocouple was immersed in mineral oil and the temperature was controlled by a homemade temperature control unit coupled to the spectrometer. The microwave power and central field were set to 10 milliwatt and 3,265 G, respectively. Spectra were acquired with a time constant of 128 ms during 240 s and with a modulation amplitude of 0.5 or 1.0 G, depending on the spin-labeled lipid. Nonlinear least-squares simulations of selected ESR spectra were performed using the Multicomponent LabVIEW (National Instruments) software, providing information on the rotational diffusion rates and order parameters of the lipids in the absence and presence of the protein. Details of the spectral simulations can be found elsewhere (48, 49).

B. subtilis lipids isolation

B. subtilis PY79 cells cultures (1000 ml) grown in Luria-Bertani medium at 37 °C (250 rpm) or after a cold shock treatment (37 to 20 °C) were harvested by centrifugation (6000 × g, 15 min). The cold shock was performed as a rapid transfer of cul-

tures from 37 to 20 °C during the mid-exponential phase of culture growth. Then, total lipids were isolated overnight at −20 °C using chloroform-methanol (1:2) protocol (50). The supernatant was removed into a clean tube and the phases were separated by adding 1 volume of chloroform (equal to the volume of chloroform in initial extraction solution) and the same volume of distilled water. After vigorous shaking for 1 min the mixture was centrifuged (3000 × *g*, 5 min). The upper methanol-water phase was discarded and the lower chloroform phase was removed to a clean glass tube, evaporated using a N_2 flow and placed into a vacuum desiccator for at least 2 h to remove traces of organic solvent.

DSC measurements

The phase transition temperature of lipid bilayer vesicles, composed of total membrane lipids extracted from *B. subtilis* PY79, was analyzed by monitoring the thermotropic phase behavior of lipid vesicles samples using DSC. Unilamellar liposomes were prepared as described above. The lipid film was hydrated in 25 mM HEPES, pH 7.5, 300 mM NaCl at about 10 mg/ml. The sample cell was filled with 500 μl of lipid vesicles suspension in the same buffer. The sample and reference cells were sealed and thermally equilibrated for about 10 min at 5 °C. Heating scans were collected in the range of 6 − 30 °C at the scan rate of 1 °C min^{-1} in a VP-DSC MicroCal MicroCalorimeter (Microcal, Northampton, MA). The reference scan was subtracted from the sample scan and the analyses of the heat capacity curves were performed using Microcal Origin software (OriginLab Corp., Northampton, MA). The measurements were repeated at least twice for two independently prepared samples.

Molecular docking calculations

The crystal structures of PlsX (14) (PDB code 1VI1) and ACP (41) (PDB code 2X2B) from *B. subtilis* were used to interrogate the ACP-PlsX interaction by docking calculations using the ZDOCK server (ZDOCK version: ZD3.0.2), without selecting residues to restrict the search (51). The docking of 4′-phosphopantetheine myristate into PlsX was carried out using the dimeric form of PlsX from *B. subtilis* (14) (PDB code 1VI1) generated in UCSF-chimera (52). The ligand was generated in PDB format using PRODRG (53) and then converted to mol2 file. The docking prediction was performed in the protein-small molecule docking server SwissDock (54).

Multiple sequence alignment

The multiple sequence alignment was performed using UNI-PROT online service using Clustal Omega (1.2.4). Alignment was assigned to structures using UCSF-chimera. The following sequences were retrieved from UNIPROT: *B. subtilis* P71018, *E. faecalis* Q82ZE8, *Clostridium tetani* Q895N0, *Lactobacillus gasseri* Q044F9, *Streptococcus pyogenes* Q5XEF9, *Pseudomonas putida* A5W716, *Mycoplasma mycoides* Q6MTC8, *Bacillus licheniformis* Q65JQ9, *Campylbacter hominis* A7I3D5, *Bacillus cereus* B7IUL2, *Clostridium botulinum* B1II87, *Helicobacter pylori* O24993, *Pseudomonas aeruginosa* Q9HZN5, *Listeria monocytogenes* Q8Y688, *Streptococcus pyogenes* P65742, and *Pasteurella multocida* P57976.

References

1. Escribá, P. V., Gonz á lez-Ros, J. M., Goñi, F. M., Kinnunen, P. K., Vigh, L., Sánchez-Magraner, L., Fernández, A. M., Busquets, X., Horváth, I., and Bárcelo-Coblijn, G. (2008) Membranes: a meeting point for lipids, proteins and therapies. *J. Cell Mol. Med.* **12,** 829 − 875 CrossRef Medline

2. de Mendoza, D. (2014) Temperature sensing by membranes. *Ann. Rev. Microbiol.* **68,** 101–116 CrossRef

3. Lopez, D., and Koch, G. (2017) Exploring functional membrane microdomains in bacteria: an overview. *Curr. Opin. Microbiol.* **36,** 76 − 84 CrossRef

4. Sajbidor, J. (1997) Effect of some environmental factors on the content and composition of microbial membrane lipids. *Crit. Rev. Biotechnol.* **17,** 87–103 CrossRef Medline

5. Los, D. A., and Murata, N. (2004) Membrane fluidity and its roles in the perception of environmental signals. *Biochim. Biophys. Acta* **1666,** 142–157 CrossRef Medline

6. Siliakus, M. F., van der Oost, J., and Kengen, S. W. M. (2017) Adaptations of archaeal and bacterial membranes to variations in temperature, pH and pressure. *Extremophiles* **21,** 651− 670 CrossRef

7. Lu, Y. J., Zhang, Y. M., Grimes, K. D., Qi, J., Lee, R. E., and Rock, C. O. (2006) Acyl-phosphates initiate membrane phospholipid synthesis in Gram-positive pathogens. *Mol. Cell* **23,** 765–772 CrossRef Medline

8. Yao, J., and Rock, C. O. (2013) Phosphatidic acid synthesis in bacteria. *Biochim. Biophys. Acta* **1831,** 495–502 CrossRef Medline

9. Parsons, J. B., and Rock, C. O. (2013) Bacterial lipids: metabolism and membrane homeostasis. *Prog. Lipid Res.* **52,** 249 −276 CrossRef Medline

10. Paoletti, L., Lu, Y. J., Schujman, G. E., de Mendoza, D., and Rock, C. O. (2007) Coupling of fatty acid and phospholipid synthesis in *Bacillus subtilis. J. Bact.* **189,** 5816 −5824 CrossRef Medline

11. Zhang, Y. M., and Rock, C. O. (2008) Thematic review series: glycerolipids: acyltransferases in bacterial glycerophospholipid synthesis. *J. Lipid Res.* **49,** 1867 −1874 CrossRef Medline

12. Parsons, J. B., Frank, M. W., Eleveld, M. J., Schalkwijk, J., Broussard, T. C., de Jonge, M. I., and Rock, C. O. (2015) A thioesterase bypasses the requirement for exogenous fatty acids in the plsX deletion of *Streptococcus pneumoniae. Mol. Microbiol.* **96,** 28 − 41 CrossRef Medline

13. Sastre, D. E., Bisson-Filho, A., de Mendoza, D., and Gueiros-Filho, F. J. (2016) Revisiting the cell biology of the acyl-ACP:phosphate transacylase PlsX suggests that the phospholipid synthesis and cell division machineries are not coupled in *Bacillus subtilis. Mol. Microbiol.* **100,** 621− 634 CrossRef Medline

14. Badger, J., Sauder, J. M., Adams, J. M., Antonysamy, S., Bain, K., Bergseid, M. G., Buchanan, S. G., Buchanan, M. D., Batiyenko, Y., Christopher, J. A., Emtage, S., Eroshkina, A., Feil, I., Furlong, E. B., Gajiwala, K. S., Gao, X., He, D., *et al*. (2005) Structural analysis of a set of proteins resulting from a bacterial genomics project. *Proteins* **60,** 787–796 CrossRef Medline

15. Kim, Y., Li, H., Binkowski, T. A., Holzle, D., and Joachimiak, A. (2009) Crystal structure of fatty acid/phospholipid synthesis protein PlsX from *Enterococcus faecalis*. *J. Struct. Funct. Genomics* **10,** 157–163 CrossRef

16. Müller, A., Wenzel, M., Strahl, H., Grein, F., Saaki, T. N. V., Kohl, B., Siersma, T., Bandow, J. E., Sahl, H. G., Schneider, T., and Hamoen, L. W. (2016) Daptomycin inhibits cell envelope synthesis by interfering with fluid membrane microdomains. *Proc. Natl. Acad. Sci. U.S.A.* **113,** E7077–E7086 CrossRef Medline

17. Loew, C., Riske, K. A., Lamy, M. T., and Seelig, J. (2011) Thermal phase behavior of DMPG bilayers in aqueous dispersions as revealed by ^{2}H- and ^{31}P-NMR. *Langmuir* **27,** 10041–10049 CrossRef Medline

18. Hawco, M. W., Coolbear, K. P., Davis, P. J., and Keough, K. M. (1981) Exclusion of fluid lipid during compression of monolayers of mixtures of dipalmitoylphosphatidylcholine with some other phosphatidylcholines. *Biochim. Biophys. Acta* **646,** 185–187 CrossRef Medline

19. Marsh, D. (1996) Components of the lateral pressure in lipid bilayers deduced from HII phase dimensions. *Biochim. Biophys. Acta* **1279,** 119–123 CrossRef Medline

20. Söderlund, T., Alakoskela, J. M., Pakkanen, A. L., and Kinnunen, P. K. (2003) Comparison of the effects of surface tension and osmotic pressure on the interfacial hydration of a fluid phospholipid bilayer. *Biophys. J.* **85,** 2333–2341 CrossRef Medline

21. Zhao, H., Sood, R., Jutila, A., Bose, S., Fimland, G., Nissen-Meyer, J., and Kinnunen, P. K. (2006) Interaction of the antimicrobial peptide pheromone Plantaricin A with model membranes: implications for a novel mechanism of action. *Biochim. Biophys. Acta* **1758,** 1461–1474 CrossRef Medline

22. Calvez, P., Demers, E., Boisselier, E., and Salesse, C. (2011) Analysis of the contribution of saturated and polyunsaturated phospholipid monolayers to the binding of proteins. *Langmuir* **27,** 1373–1379 CrossRef Medline

23. Boisselier, É., Calvez, P., Demers, É., Cantin, L., and Salesse, C. (2012) Influence of the physical state of phospholipid monolayers on protein binding. *Langmuir* **28,** 9680–9688 CrossRef Medline

24. Marsh, D., and Horváth, L. I. (1998) Structure, dynamics and composition of the lipid-protein interface: perspectives from spin-labelling. *Biochim. Biophys. Acta* **1376,** 267–296 CrossRef Medline

25. Borbat, P. P., Costa-Filho, A. J., Earle, K. A., Moscicki, J. K., and Freed, J. H. (2001) Electron spin resonance in studies of membranes and proteins. *Science* **291,** 266–269 CrossRef Medline

26. Basso, L. G. M., Mendes, L. F. S., and Costa-Filho, A. J. (2016) The two sides of a lipid-protein story. *Biophys. Rev.* **8,** 179–191 CrossRef Medline

27. Bartucci, R. (2013) *Spin-Labeling EPR of Lipid Membranes*, Springer, Berlin CrossRef

28. Beranová, J., Mansilla, M. C., de Mendoza, D., Elhottová, D., and Konopásek, I. (2010) Differences in cold adaptation of *Bacillus subtilis* under anaerobic and aerobic conditions. *J. Bacteriol.* **192,** 4164–4171 CrossRef Medline

29. Altabe, S. G., Aguilar, P., Caballero, G. M., and de Mendoza, D. (2003) The *Bacillus subtilis* acyl lipid desaturase is a Δ5 desaturase. *J. Bacteriol.* **185,** 3228–3231 CrossRef Medline

30. Marsh, D. (1981) Electron spin resonance: spin labels. in *Molecular biology biochemistry and biophysics: membrane spectroscopy* (Grell, E., ed) Vol. 31, pp. 51–142, Springer, Berlin CrossRef

31. Whited, A. M., and Johs, A. (2015) The interactions of peripheral membrane proteins with biological membranes. *Chem. Phys. Lipids* **192,** 51–59 CrossRef Medline

32. Luckey, M. (2008) *Membrane Structural Biology: with Biochemical and Biophysical Foundation*, Cambridge University Press, Cambridge

33. Seelig, J. (2004) Thermodynamics of lipid-peptide interactions. *Biochim. Biophys. Acta* **1666,** 40–50 CrossRef Medline

34. Bryan, P. N., and Orban, J. (2010) Proteins that switch folds. *Curr. Opin. Struct. Biol.* **20,** 482–488 CrossRef Medline

35. Lella, M., and Mahalakshmi, R. (2017) Metamorphic proteins: emergence of dual protein folds from one primary sequence. *Biochemistry* **56,** 2971–2984 CrossRef Medline

36. Jiang, Y., Dai, X., Qin, M., and Guo, Z. (2019) Identification of an amphipathic peptide sensor of the *Bacillus subtilis* fluid membrane microdomains. *Commun. Biol.* **2,** 316 CrossRef Medline

37. McAllister, K. A., Peery, R. B., and Zhao, G. (2006) Acyl carrier protein synthases from Gram-negative, Gram-positive, and atypical bacterial species: biochemical and structural properties and physiological implications. *J. Bacteriol.* **188,** 4737–4748 CrossRef Medline

38. Maloney, F. P., Gerwick, L., Gerwick, W. H., Sherman, D. H., and Smith, J. L. (2016) Anatomy of the β-branching enzyme of polyketide biosynthesis and its interaction with an acyl-ACP substrate. *Proc. Natl. Acad. Sci. U.S.A.* **113,** 10316–10321 CrossRef Medline

39. Zhang, L., Xiao, J., Xu, J., Fu, T., Cao, Z., Zhu, L., Chen, H. Z., Shen, X., Jiang, H., and Zhang, L. (2016) Crystal structure of FabZ-ACP complex reveals a dynamic seesaw-like catalytic mechanism of dehydratase in fatty acid biosynthesis. *Cell Res.* **26,** 1330–1344 CrossRef Medline

40. Agarwal, V., Lin, S., Lukk, T., Nair, S. K., and Cronan, J. E. (2012) Structure of the enzyme-acyl carrier protein (ACP) substrate gatekeeper complex required for biotin synthesis. *Proc. Natl. Acad. Sci. U.S.A.* **109,** 17406–17411 CrossRef Medline

41. Cryle, M. J., and Schlichting, I. (2008) Structural insights from a P450 Carrier Protein complex reveal how specificity is achieved in the P450(BioI) ACP complex. *Proc. Natl. Acad. Sci. U.S.A.* **105,** 15696–15701 CrossRef Medline

42. Babu, M., Greenblatt, J. F., Emili, A., Strynadka, N. C., Reithmeier, R. A., and Moraes, T. F. (2010) Structure of a SLC26 anion transporter STAS domain in complex with acyl carrier protein: implications for *E. coli* YchM in fatty acid metabolism. *Structure* **18,** 1450–1462 CrossRef Medline

43. Cronan, J. E. (2014) The chain-flipping mechanism of ACP (acyl carrier protein)-dependent enzymes appears universal. *Biochem. J.* **460,** 157–163 CrossRef Medline

44. Martinez, M. A., Zaballa, M. E., Schaeffer, F., Bellinzoni, M., Albanesi, D., Schujman, G. E., Vila, A. J., Alzari, P. M., and de Mendoza, D. (2010) A novel role of malonyl-ACP in lipid homeostasis. *Biochemistry* **49,** 3161–3167 CrossRef Medline

45. Saita, E. A., and de Mendoza, D. (2015) Thermosensing via transmembrane protein-lipid interactions. *Biochim. Biophys. Acta* **1848,** 1757–1764 CrossRef Medline

46. Morozova, D., Guigas, G., and Weiss, M. (2011) Dynamic structure formation of peripheral membrane proteins. *PLoS Comp. Biol.* **7,** e1002067 CrossRef

47. Takada, H., Fukushima-Tanaka, S., Morita, M., Kasahara, Y., Watanabe, S., Chibazakura, T., Hara, H., Matsumoto, K., and Yoshikawa, H. (2014) An essential enzyme for phospholipid synthesis associates with the *Bacillus subtilis* divisome. *Mol. Microbiol.* **91,** 242–255 CrossRef Medline

48. Basso, L. G., Vicente, E. F., Crusca, E., Jr, Cilli, E. M., and Costa-Filho, A. J. (2016) SARS-CoV fusion peptides induce membrane surface ordering and curvature. *Sci. Rep.* **6,** 37131 CrossRef Medline

49. Budil, D. E., Sale, K. L., Khairy, K. A., and Fajer, P. G. (2006) Calculating slow-motional electron paramagnetic resonance spectra from molecular dynamics using a diffusion operator approach. *J. Phys. Chem. A* **110,** 3703–3713 CrossRef Medline

50. Bligh, E. G., and Dyer, W. J. (1959) A rapid method of total lipid extraction and purification. *Can. J. Biochem. Physiol.* **31,** 911–917 Medline

51. Pierce, B. G., Wiehe, K., Hwang, H., Kim, B. H., Vreven, T., and Weng, Z. (2014) ZDOCK server: interactive docking prediction of protein-protein complexes and symmetric multimers. *Bioinformatics* **30,** 1771–1773 CrossRef Medline

52. Pettersen, E. F., Goddard, T. D., Huang, C. C., Couch, G. S., Greenblatt, D. M., Meng, E. C., and Ferrin, T. E. (2004) UCSF Chimera: a visualization system for exploratory research and analysis. *J. Comput. Chem.* **25,** 1605–1612 CrossRef Medline

53. Schüttelkopf, A. W., and van Aalten, D. M. (2004) PRODRG: a tool for high-throughput crystallography of protein-ligand complexes. *Acta Crystallogr. D Biol. Crystallogr.* **60,** 1355–1363 CrossRef Medline

54. Grosdidier, A., Zoete, V., and Michielin, O. (2011) SwissDock, a protein-small molecule docking web service based on EADock DSS. *Nucleic Acids Res.* **39,** W270–W277 CrossRef Medline

55. Sastre, D. E., Pulschen, A. A., Basso, L. G. M., Benites Pariente, J. S., Marques Netto, C. G. C., Machinandiarena, F., Albanesi, D., Navarro, M. V. A. S., de Mendoza, D., Gueiros-Filho, F. J. (2019) The phosphatidic-acid pathway enzyme PlsX plays both catalytic and channeling roles in bacterial phospholipid synthesis. *J. Biol. Chem.* **295,** 2148–2159 CrossRef Medline